



Revisiting the Strongest Martian X-Ray Halo Observed by *XMM-Newton* on 2003 November 19–21

Limei Yan^{1,2} , Jiawei Gao¹, Lihui Chai^{1,2,3} , Lingling Zhao⁴ , Zhaojin Rong^{1,2,3}, and Yong Wei^{1,2,3}

¹ Key Laboratory of Earth and Planetary Physics, Institute of Geology and Geophysics, Chinese Academy of Sciences, Beijing 100029, People's Republic of China; chailihui@mail.iggcas.ac.cn

² Beijing National Observatory of Space Environment, Institute of Geology and Geophysics, Chinese Academy of Sciences, Beijing, People's Republic of China

³ College of Earth Science, University of Chinese Academy of Sciences, Beijing, People's Republic of China

⁴ Center for Space Plasma and Aeronomic Research (CSPAR), University of Alabama in Huntsville, Huntsville, AL 35805, USA

Received 2019 July 1; revised 2019 August 30; accepted 2019 September 2; published 2019 September 27

Abstract

On 2003 November 20–21, when the most intense geomagnetic storm during solar cycle 23 was observed at Earth, *XMM-Newton* recorded the strongest Martian X-ray halo hitherto. The strongest Martian X-ray halo has been suggested to be caused by the unusual solar wind, but no direct evidence has been given in previous studies. Here, we examined the Mars Global Surveyor (MGS) observations and found unambiguous evidence of unusual solar wind impact during that *XMM-Newton* observation: the whole induced magnetosphere of Mars was highly compressed. By comparing the solar wind dynamic pressure estimated at Mars from MGS observation and that predicted by different solar wind propagation models, it is further supported that the interplanetary condition during the *XMM-Newton* observation is not related to the quiet solar wind, but to solar wind disturbances with enhanced dynamic pressure, which is probably related to the interplanetary coronal mass ejection observed at Earth on 2003 November 20. A solar energetic particle event also impacted Mars during the *XMM-Newton* observation and lasted for several days. Its impact on the production of the X-ray emission from Mars may be worth investigating in the future.

Unified Astronomy Thesaurus concepts: Solar coronal mass ejections (310); Mars (1007); Planetary atmospheres (1244); X-ray astronomy (1810); Exosphere (499)

1. Introduction

In the past two decades, it has been established that the neutral particles in an unmagnetized planetary exosphere can interact with the highly charged solar wind heavy ions, and this process produces X-ray emission (Dennerl 2010). The observation of X-rays from Mars provides useful information on the exospheric processes on a global scale, which is important for understanding the present state of the Martian atmosphere and its evolution. The X-rays from this process usually form as a halo around Mars. The Martian X-ray halo was first detected by *Chandra* on 2001 July 4 and found to be extended to 3 Mars radii with a total luminosity of 0.5 ± 0.2 MW in the energy range 0.5–1.2 keV (Dennerl 2002). The Martian X-ray halo observed by *XMM-Newton* on 2003 November 19–21 extended up to 8 Mars radii with a luminosity of 12.8 ± 1.4 MW in the energy range 0.365–0.88 keV (Dennerl et al. 2006), which is much stronger than that observed by *Chandra*. The observations of *Chandra* and *XMM-Newton* were both conducted during the solar maximum. In contrast, the X-ray observation of Mars by Suzaku on 2008 April 3–5 during the solar minimum did not detect any significant X-ray halo (Ishikawa et al. 2011). Therefore, the Martian X-ray halo observed by *XMM-Newton* is the strongest ever observed. The flux of the Martian X-ray halo observed by *XMM-Newton* was found to be highly variable including several outbursts (Dennerl 2006). Observational evidence suggests that this event is unusual and may be subject to space weather effects.

The drivers of this event still remain unclear, mainly because there was no solar wind monitor available in the upstream of Mars. Dennerl et al. (2006) first proposed that this event was caused by some unusual solar activity. Indeed, an extremely

strong interplanetary coronal mass ejection (ICME) impacted Earth on 2003 November 20–21, causing the most intense geomagnetic storm during solar cycle 23, and producing some unexpected phenomena of magnetosphere–ionosphere coupling never observed before (e.g., Wei et al. 2012). During that time, the longitudinal separation between Earth and Mars was around 30° . As suggested by Opitz et al. (2010), for the solar minimum, it is reliable to extrapolate solar wind from measurements in Earth's orbit to Mars's orbit as long as the longitudinal separation is less than 65° . However, it is not known whether this method may be applied for the solar maximum, especially for coronal mass ejection (CME) propagation. Koutroumpa et al. (2012) shifted and scaled the usual solar wind parameters on 2003 November 18–19 before the arrival of the ICME from Earth's orbit to Mars's orbit, and used them to simulate X-ray emission from Mars, but they found the simulated X-ray emission level was far lower than in the *XMM-Newton* observations. One possible reason is that the current modeling methods may have some problems (Ali et al. 2010). Another possibility, the strongest X-ray emission is due to the impact of solar wind disturbances instead of the usual solar wind that was used by Koutroumpa et al. (2012) in simulating the X-ray emission.

Here we present unambiguous evidence for the impact of solar wind disturbances with enhanced dynamic pressure during *XMM-Newton* observation based on Mars Global Surveyor (MGS) observation. The observational evidence suggests that the solar wind disturbances at Mars is probably related to the ICME observed at Earth on 2003 November 20–21.

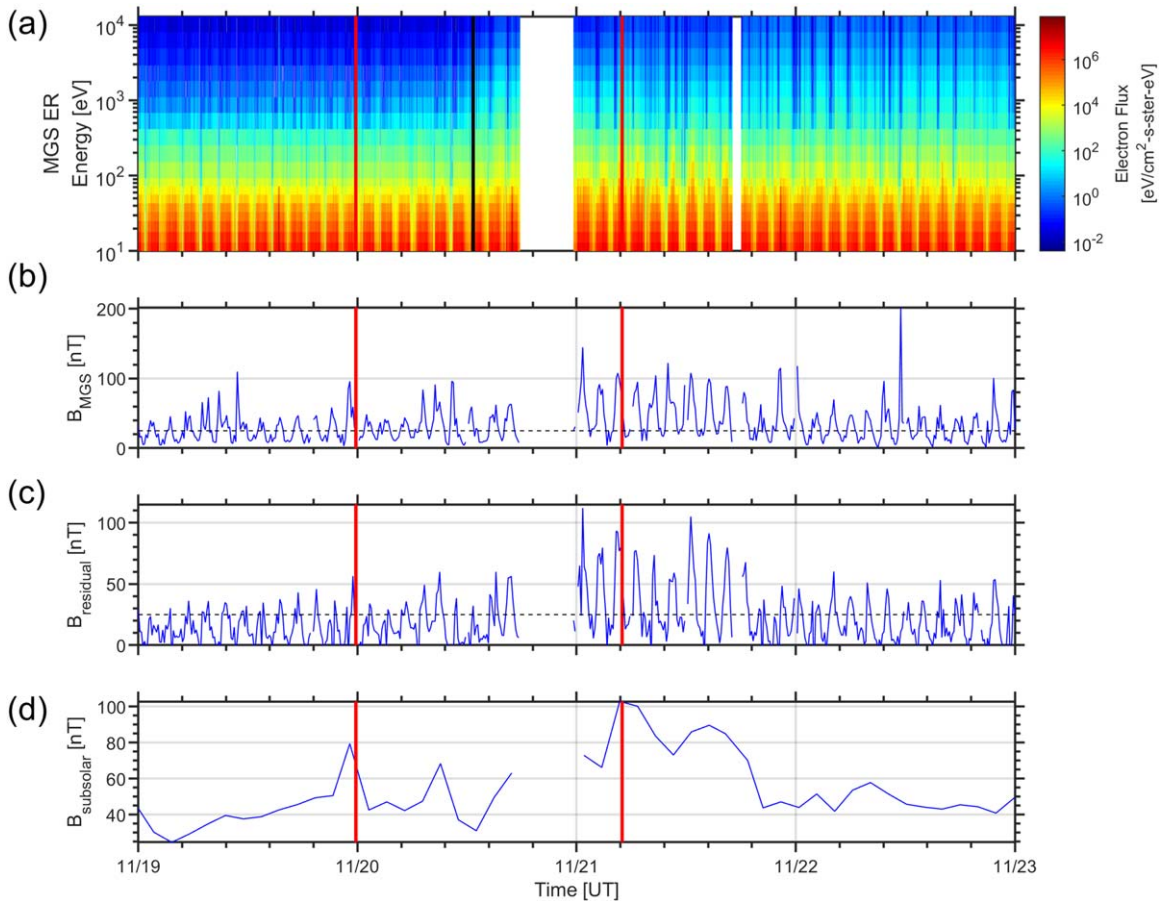


Figure 1. Panel (a): the electron energy spectrum obtained by ER on board MGS. Panel (b): the magnetic field intensity observed by MGS. Panel (c): the residual magnetic field (the magnetic field observed by MGS minus the crustal magnetic field from the Morschhauser model). The dashed line shows a magnetic field intensity of 25 nT. Panel (d): the subsolar magnetic field strength of the piled-up region at 400 km altitude above Mars estimated by Brain et al. (2005) based on the MGS observation. The time interval of *XMM-Newton* observation is labeled by the red vertical lines. The arrival of SEP is labeled by the black vertical line in panel (a). The magnetic fields shown in panels (b) and (c) are at a time resolution of 10 minutes.

2. Observation and Results

2.1. Instrumentation

The MGS spacecraft was inserted into its orbit in March of 1999, with a maximum altitude of 400 km. The instruments on board MGS consist of two redundant triaxial fluxgate magnetometers (MAG) and an electron reflectometer (ER; Acuña et al. 1992; Acuña et al. 1998). The fluxgate magnetometers on board MGS provide fast vector measurements with up to 32 samples s^{-1} (Acuña et al. 2001). The MGS ER is a hop hat electrostatic analyzer that measured superthermal electrons in the energy channels ranging from 10 eV to 20 keV (Mitchell et al. 2001). Even though the ER was originally designed to detect low-energy electrons, it can also measure energetic particles with energies higher than 30 MeV (Delory et al. 2012).

2.2. Compression of the Whole Induced Magnetosphere

To study what happened in the time interval of the *XMM-Newton* observation, the time evolution of the magnetic field and electron energy spectrum was investigated. The time interval for the *XMM-Newton* observation is from 23:48:58 UT on 2003 November 19 to 04:58:53 UT on 2003 November 21 (labeled by the red vertical lines in Figure 1). The magnetic field observed by MGS shows a significant increase from 2003

November 21 00:48:24 UT to 2003 November 21 20:25 UT (Figure 1(b)). Unfortunately, there is a large data gap from 2003 November 20 16:53:09 UT to 2003 November 21 00:48:24 UT, so that the actual beginning of the strong increase of the magnetic field cannot be decided and may range between 2003 November 20 16:53:09 UT and 2003 November 21 00:48:24 UT. The recorded Martian magnetic fields are mainly composed of a draping magnetic field, which is contributed by the solar wind interaction with Mars and the crustal magnetic field. In order to investigate whether the increase of magnetic field strength is contributed by the compression of solar wind or the crossing of the crustal magnetic field, the residual magnetic field (the magnetic field observed by MGS minus the crustal magnetic field from the Morschhauser model; Morschhauser et al. 2014) is shown in Figure 1(c). The residual magnetic field illustrates that the significant increase of the magnetic field is owing to the high compression of the whole induced magnetosphere of Mars instead of crossing the Martian crustal magnetic field. The compression of the whole induced magnetosphere of Mars has been shown as a feature of the Martian ionosphere’s response to ICME impact (e.g., Crider et al. 2005; Morgan et al. 2014). The subsolar magnetic field strength of the piled-up region at 400 km altitudes above Mars

given by Brain et al. (2005),⁵ which can be used as a proxy to see the variation of the solar wind dynamic pressure, shows a significant increase indicating that the solar wind dynamic pressure was increased from 2003 November 21 00:48:24 UT to 2003 November 21 22:00 UT (Figure 1(d)). This observational evidence suggests that Mars was impacted not by quiet solar wind but by solar wind disturbances with enhanced dynamic pressure during the *XMM-Newton* observation.

During the *XMM-Newton* observation, a solar energetic particle (SEP) event arrived at Mars at 12:40 UT on 2003 November 20 (labeled by the black vertical line in Figure 1(a)) lasting for several days, which was identified by Delory et al. (2012). The SEP is caused by a flare erupted on the Sun at 07:36 UT on 2003 November 20, and its corresponding CME was detected by *Solar and Heliospheric Observatory (SOHO)*/LASCO at 08:06 UT on 2003 November 20. After the arrival of SEP, the high-energy electron flux shows a significant increase lasting for several days.

2.3. Discussion

To investigate if the observed solar wind disturbances with enhanced dynamic pressure are related to the ICME observed at Earth, the comparison between the solar wind dynamic pressure estimated at Mars and that predicted by solar wind propagation model was conducted. The upstream solar wind dynamic pressure of Mars can be evaluated by assuming a balance between the incident solar wind dynamic pressure and the magnetic field pressure in the magnetic pileup region (Crider et al. 2003). Here, the solar wind dynamic pressure (P_{sw}) is estimated by $B^2/(2\mu_0)$, where B is the subsolar magnetic field strength shown in Figure 1(d) and μ_0 is the magnetic permeability in the vacuum.

The P_{sw} at Mars can be calculated with P_{sw} observed near Earth based on the solar wind propagation models. The propagation models for the quiet solar wind coming from a continuous source region consider both the angular and radial separations between Earth and Mars, such as the Tao model (Tao et al. 2005). The propagation models for the impulsive solar wind events consider only the radial separation, such as the Crider model (Crider et al. 2005). The Tao model simulates a one-dimensional magnetohydrodynamic (MHD) propagation of the solar wind. The Crider model simply scales the P_{sw} by a radial scaling of r^{-2} and shifts the P_{sw} from Earth's orbit to Mars's orbit by the time lag $dt = (r_M - r_E)/v_E$, where r is the heliocentric distance, v is the solar wind speed that is assumed constant, and the subscripts M and E stand for Mars and Earth, respectively. The inputs of the two models are the hourly solar wind parameters from OMNI.⁶ The P_{sw} at Mars calculated by the Tao model can be accessed at AMDA. For the Crider model, we scaled and shifted the P_{sw} around the ICME interval from Earth's orbit to Mars's orbit using the time lag estimated by $(r_M - r_E)/v_E$, where v_E is the maximum speed during each ICME.

The P_{sw} at Mars from 2003 October 20 to 2003 December 8, estimated by MGS observation and predicted by the two different propagation models, are shown in Figure 2. During the time interval shown here, the longitudinal separation

between Earth and Mars is less than 40° (Figure 2(d)). The ICMEs at Earth identified by Jian et al. (2006) are labeled by the gray filled rectangles in Figure 2(a). For the quiet solar wind, the P_{sw} at Mars predicted by the Tao model agrees well with that estimated at Mars (Figure 2(b)). Even though the Crider model is more suitable for wide impulsive events like ICMEs, sometimes the predicted arrival time and the P_{sw} magnitude of ICMEs do not agree well with that estimated at Mars (Figure 2(c)). This is because both the propagation and the structure of ICMEs are three-dimensionally anisotropic. Only when the propagation speed and the structure of ICMEs are similar at the direction of Earth and Mars do the predicted arrival time and magnitude of the P_{sw} agree well with that estimated at Mars.

The ICME arrived at Earth on 2003 November 20, the ninth ICME (ICME9) in Figure 2(a), and is a candidate origin of the solar wind disturbances with enhanced dynamic pressure at Mars during the *XMM-Newton* observation. As predicted by the Tao model, the quiet solar wind before the ICME9 arrived at Mars before the *XMM-Newton* observation (Figure 3(a)). For the quiet solar wind before and after the *XMM-Newton* observation as highlighted by the light yellow shaded regions in Figure 3(a), the predicted P_{sw} agree well with that estimated at Mars. In contrast, around the *XMM-Newton* observation, the predicted P_{sw} is very different from that estimated at Mars. The simplest Ballistic model (e.g., Riley & Lionello 2011; Dósa et al. 2018 and references therein), the result of which is not given in this Letter, shows similar results as that from the Tao model. This suggests that the solar wind disturbances with enhanced P_{sw} at Mars are not related to the quiet solar wind.

To investigate the relation between the solar wind disturbances at Mars and the ICME9 at Earth, the predicted and the observed arrival times of the P_{sw} enhancement are compared. The predicted arrival time of the ICME9 from the Crider model is later than that observed at Mars for 13.5–21.5 hr (Figure 2(c)). This delay is not unusual. The predicted arrival time of ICME2 (the second ICME in Figure 2(a)) is also later than that observed at Mars for ~ 17.5 hr (Figure 2(c)). A delay of 10–20 hr between the predicted and observed arrival times also usually appears for the shocks or dynamic pressure enhancements in previous studies (e.g., Tao et al. 2005; Zieger & Hansen 2008). Zieger & Hansen (2008) suggested that there might be an additional unknown acceleration mechanism for shocks that is not included in the existing solar wind propagation model. Thus, it is difficult to determine whether the solar wind disturbances observed at Mars are related to ICME9 at Earth. To further investigate the relation between the solar wind disturbances at Mars and the ICME9 at Earth, the predicted P_{sw} are shifted earlier to compare with the P_{sw} estimated at Mars. The predicted P_{sw} of ICME2 and ICME9 were shifted earlier by 17.5 hr and 19.5 hr, respectively. The shifted predicted P_{sw} is consistent with that estimated at Mars (Figures 3(b) and (c)). Even though there is a large data gap for ICME9, the predicted P_{sw} beyond the data gap agrees well with that estimated at Mars (Figure 3(a)). The evidence above suggests that the solar wind disturbances with enhanced dynamic pressure at Mars during the *XMM-Newton* observation is probably related to the ICME observed at Earth on 2003 November 20.

⁵ The subsolar magnetic field strength given by Brain et al. can be obtained from Automated Multi-Data Set Analysis (AMDA) and <http://sprg.ssl.berkeley.edu/~brain/proxies/subsolfield.html>.

⁶ The data used here were downloaded from <https://cdaweb.sci.gsfc.nasa.gov/index.html/>.

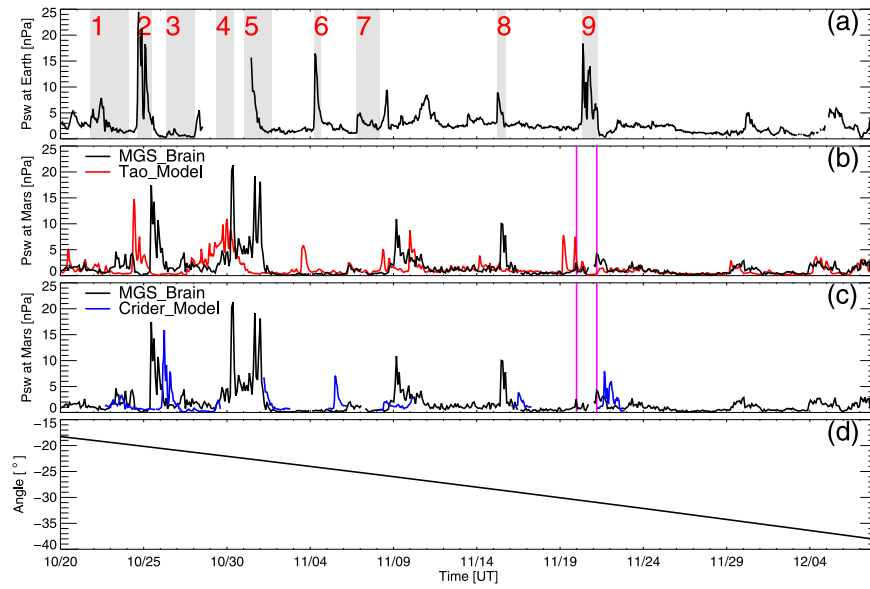


Figure 2. Panel (a): the P_{sw} at Earth from OMNI. The light gray filled rectangles label the ICMEs at Earth identified by Jian et al. (2006). Panels (b)–(c): the P_{sw} estimated from the MGS observation (dark curves) and that predicted by different solar wind propagation models. Red curves in panel (b) show results from the Tao model. Blue curves in panel (c) show results from the Crider model. Panel (d): the Earth–Sun–Mars angle. The time interval of *XMM-Newton* observation is labeled by pink vertical lines.

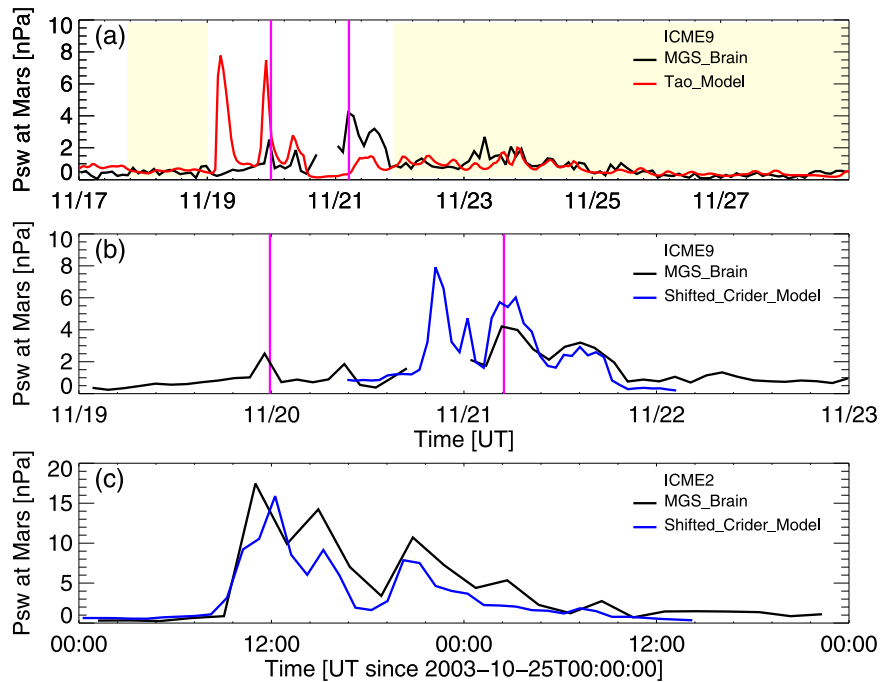


Figure 3. Panel (a): the P_{sw} estimated from MGS observation (black curve) and the predicted P_{sw} from the Tao model (red curve). The yellow filled rectangles highlight the time intervals before and after the *XMM-Newton* observation when the predicted P_{sw} agree well with that estimated from MGS observation. Panel (b): the P_{sw} estimated from MGS observation (black curve) and the predicted P_{sw} from the Crider model that is shifted earlier by 19.5 hr (blue curve) for ICME9 in Figure 2(a). Panel (c): similar to panel (b), but for the results of ICME2 labeled in Figure 2(a). The predicted P_{sw} from the Crider model is shifted earlier by 17.5 hr (blue curve). The time interval of *XMM-Newton* observation is labeled by pink vertical lines.

3. Summary

In this Letter, based on the MGS observation we found significant compression of the whole induced magnetosphere of Mars during the *XMM-Newton* observation, illustrating that the strongest X-ray halo of Mars recorded by *XMM-Newton* is owing to the impact of solar wind disturbances with enhanced dynamic pressure. This kind of event, as shown in this Letter, is frequently occurring as a consequence of the solar wind

disturbances (such as stream interaction region and ICME) impact. Based on the MGS observation, the average occurrence rate of such events (a peak orbital averaged residual magnetic intensity larger than 50 nT) is $\sim 58 \text{ yr}^{-1}$ during the maximum and early declining phase of solar cycle 23 (Vennerstrom 2011). Based on the Mars Express (MEX) observation, the occurrence rate of such events at the solar minimum is $\sim 35 \text{ yr}^{-1}$ (Edberg et al. 2010), which is lower than that at the solar maximum. Like Mars, Venus has a similar induced magnetosphere due to

the lack of a global dipole field. The strong compression of the whole induced magnetosphere of Venus as a response to the solar wind disturbances is also frequently occurring (e.g., Edberg et al. 2011; Vech et al. 2015; Futaana et al. 2017; Xu et al. 2019). The occurrence rate of such an event on Venus during the solar minimum is $\sim 32 \text{ yr}^{-1}$ (Edberg et al. 2011), which is similar to that on Mars.

By detailed comparisons of the solar wind dynamic pressure estimated at Mars with that predicted from solar wind propagation models, we further provide evidence that the solar wind disturbances with enhanced dynamic pressure during the *XMM-Newton* observation are not the usual solar wind but possibly the corresponding feature of the ICME observed at Earth on 2003 November 20. Therefore, it is not precise to use the quiet solar wind from 2003 November 18 to 19 observed at Earth to estimate the X-ray emission from Mars, as conducted by Koutroumpa et al. (2012).

Even though the observational evidence suggests that the ICME observed at Earth on 2003 November 20 is the possible origin of the solar wind disturbances at Mars, the possibility of other ICMEs or stream interaction regions (SIRs) could not be fully excluded. First, the ejecta of the ICME observed at Earth were not detected by *SOHO/LASCO* (Grechnev et al. 2014), so it is impossible to see if the ICME observed at Earth can arrive at Mars from the ICME propagation model. Second, there are no direct magnetic field and plasma observations in the solar wind at Mars or other in situ observations in the direction of Mars, thus it is not possible to know whether there is other ICMEs or SIRs which can lead to the enhancement of P_{sw} at Mars.

Furthermore, an SEP event also impacted Mars during the *XMM-Newton* observation and lasted for several days. The abundance of heavy ions during the SEP event is different from that in the quiet solar wind, and whether it could also influence the production of the X-ray emission from Mars or not is worth investigating in future.


The work is supported by the Strategic Priority Research Program of Chinese Academy of Sciences (grant No. XDA17010201) and the National Natural Science Foundation of China (41525016, 41661164034, 41704166, 41674177, 41874208, 201774188, 41774188). L.M.Y. is supported by the National Postdoctoral Program for Innovative Talents (grant

BX201600159) and the Project funded by China Postdoctoral Science Foundation (grant 2017M610978). L.Z. acknowledges partial support from the NSF EPSCoR RII-Track-1 Cooperative Agreement OIA-1655280.

ORCID iDs

Limei Yan  <https://orcid.org/0000-0002-1402-923X>

Lihui Chai  <https://orcid.org/0000-0001-8844-9176>

Lingling Zhao  <https://orcid.org/0000-0002-4299-0490>

References

- Acuña, M. H., Connerney, J. E. P., Wasilewski, P., et al. 1992, *JGR*, **97**, 7799
- Acuña, M. H., Connerney, J. E. P., Wasilewski, P., et al. 1998, *Sci*, **279**, 1676
- Acuña, M. H., Connerney, J. E. P., Wasilewski, P., et al. 2001, *JGR*, **106**, 23403
- Ali, R., Neill, P. A., Beiersdorfer, P., et al. 2010, *ApJL*, **716**, L95
- Brain, D. A., Halekas, J. S., Lillis, R., et al. 2005, *GeoRL*, **32**, L18203
- Crider, D. H., Espley, J., Brain, D. A., et al. 2005, *JGRA*, **110**, A09S21
- Crider, D. H., Vignes, D., Krymskii, A. M., et al. 2003, *JGRA*, **108**, 1461
- Delory, G. T., Luhmann, J. G., Brain, D., et al. 2012, *SpWea*, **10**, S06003
- Dennerl, K. 2002, *A&A*, **394**, 1119
- Dennerl, K. 2006, *SSRv*, **126**, 403
- Dennerl, K. 2010, *SSRv*, **157**, 57
- Dennerl, K., Lisse, C. M., Bhardwaj, A., et al. 2006, *A&A*, **451**, 709
- Dósa, M., Opitz, A., Dálya, Z., & Szegő, K. 2018, *SoPh*, **293**, 127
- Edberg, N. J. T., Nilsson, H., Williams, A. O., et al. 2010, *GeoRL*, **37**, L03107
- Edberg, N. J. T., Nilsson, H., Futaana, Y., et al. 2011, *JGRA*, **116**, A09308
- Futaana, Y., Stenberg Wieser, G., Barabash, S., & Luhmann, J. G. 2017, *SSRv*, **212**, 1453
- Grechnev, V. V., Uralov, A. M., Chertok, I. M., et al. 2014, *SoPh*, **289**, 4653
- Ishikawa, K., Ezoe, Y., Ohashi, T., Terada, N., & Futaana, Y. 2011, *PASJ*, **63**, S705
- Jian, L., Russell, C. T., Luhmann, J. G., & Skoug, R. M. 2006, *SoPh*, **239**, 393
- Koutroumpa, D., Modolo, R., Chanteur, G., et al. 2012, *A&A*, **545**, A153
- Mitchell, D. L., Lin, R. P., Mazelle, C., et al. 2001, *JGR*, **106**, 23419
- Morgan, D. D., Diéval, C., Gurnett, D. A., et al. 2014, *JGRA*, **119**, 5891
- Morschhauser, A., Lesur, V., & Grott, M. 2014, *JGRE*, **119**, 1162
- Opitz, A., Fedorov, A., Wurz, P., et al. 2010, *SoPh*, **264**, 377
- Riley, P., & Lionello, R. 2011, *SoPh*, **270**, 575
- Tao, C., Kataoka, R., Fukunishi, H., Takahashi, Y., & Yokoyama, T. 2005, *JGRA*, **110**, A11208
- Vech, D., Szego, K., Opitz, A., et al. 2015, *JGRA*, **120**, 4613
- Vennerstrom, S. 2011, *Icar*, **215**, 234
- Wei, Y., Wan, W., Zhao, B., et al. 2012, *JGRA*, **117**, A09308
- Xu, Q., Xu, X., Chang, Q., et al. 2019, *ApJ*, **876**, 84
- Zieger, B., & Hansen, K. C. 2008, *JGRA*, **113**, A08107